Miah, Md Suzan; Heino, Mikko; Icheln, Clemens; Haneda, Katsuyuki

Design of a Reference Dipole-Loop Antenna Array at 28 GHz

Published in:
Proceedings of the European Conference on Antennas and Propagation

Published: 01/03/2019

Document Version
Peer reviewed version

Please cite the original version:
Miah, M. S., Heino, M., Icheln, C., & Haneda, K. (2019). Design of a Reference Dipole-Loop Antenna Array at 28 GHz. In *Proceedings of the European Conference on Antennas and Propagation* Article 8739385 (Proceedings of the European Conference on Antennas and Propagation). IEEE.
https://ieeexplore.ieee.org/document/8739385

Design of a Reference Dipole-Loop Antenna Array at 28 GHz

Md. Suzan Miah, Mikko Heino, Clemens Icheln, Katsuyuki Haneda
Dept. of Electronics and Nanoengineering, Aalto University-School of Electrical Engineering, Espoo FI-00076, Finland.
(e-mail: md.miah@aalto.fi)

***Abstract*—This paper proposes an array antenna at 28 GHz that can be used to measure polarimetric omni-directional pathloss. The array consists of a printed microstrip dipole and loop with an integrated tapered balun structure. The design and experimental results of low profile microstrip dipole and loop antenna show wideband matching and radiation performance. Over 6 GHz of −10 dB impedance matching bandwidth has been achieved for the dipole, whereas the loop shows 0.2 GHz ranging from 27.9 to 28.1 GHz. A fairly good agreement between the simulated and measured radiation pattern validates our simulation method. The omni-directional behaviors of both dipole and loop make it suitable as a reference antenna for over-the-air antenna testing at 28 GHz.**

***Index Terms*—electric dipole, loop antenna, mm-wave array antenna, tapered line balun.**

I. Introduction

New generations of cellular mobile networks, called the fifth-generation (5G) radios, have been studied intensively both in the industry and academy. The new generation of networks exploits radio frequencies higher than 6 GHz actively for higher peak data rates and network throughput. One of the practical issues in cellular mobile radios operating at higher frequency bands is its smaller coverage due to the higher path loss compared to the lower bands. Mathematical models and tools to predict radio propagation losses have been studied in recent years extensively, e.g., [1]. It is inevitable to employ multiple antenna elements as an array for transmitting and receiving signals in order to minimize the implications imposed by the higher pathloss at higher frequencies. Possible gains or losses attributed to array antennas implemented on mobile phone devices have not studied extensively, particularly under realistic operational conditions with the influence of head, hands, fingers and human bodies of mobile users [2]–[5].

In Multiple-input and Multiple-output (MIMO) communication systems, array gain means a power gain of transmitted signals that is achieved by using multiple-antennas at the transmitter and/or receiver, with respect to a reference case, which is facilitated using the single-element antenna in an array. Thus, the conventional array gain is practically not defined uniquely as it depends on the choice of a reference antenna element in an array. Powers from each antenna element in an array practically vary significantly depending on its polarization, orientation and element types. For a fair comparison of phased antenna arrays consisting of different element types and configurations, [5] reports a novel definition of the total array gain. It defines the total array gain as a received power at a mobile phone antenna array that it can receive from multipath radio channels with respect to omni-directional pathloss when the mobile would be equipped with an idealistic omni-directional antenna. The omni-directional pathloss has been studied extensively in mm-wave channel modeling, including the recently established 3GPP standard channel model for new radios [1]. The total array gain along with the omni-pathloss, therefore, provides the pathloss when a mobile is equipped with an antenna array. In contrast to the conventional array gain, the total array gain is uniquely defined and allows us to compare arrays formed by different antenna elements and configurations, as well as influenced by the user.

The polarimetric omni-directional pathloss can be achieved using an idealistic colocated electric and magnetic dipole as an array for vertical and horizontal polarization, respectively. However, in practice, the electric and magnetic dipole can be separated by a distance to form the array. In this paper, we composed a printed dipole and loop as an array at 28 GHz, which is considered as one of the candidate frequency bands for the 5G cellular networks. Electro-magneto antennas as array operating below 15 GHz are presented in [6]–[9], but do not to realize omni-directional radiation pattern. Printed dipole antenna solutions with microstrip tapered balun at 2.4 GHz are presented in [10]–[12]. Printed loop antennas with microstrip tapered balun for below 6 GHz are presented in [13]–[15]. According to the authors best knowledge, none of the previous studies report such electric and magnetic dipole as an array at 28 GHz that show dual-polarized omni-directional radiation pattern and serve as a reference array. In this paper, we propose an antenna array, which is a composite of a planar dipole and loop to obtain comparable E_θ and E_ϕ components of the far electric field at the azimuth plane, respectively.

The remainder of this paper is organized as follows. Section II illustrates the proposed antenna array configuration and simulations, while Section III addresses the experimental validation of the numerical results. Finally, Section IV concludes this paper.

II. Array Configuration and Numerical Results

A. Dipole and Microstrip Tapered Balun

A half-wavelength vertically polarized dipole at 28 GHz is shown in Fig. 1(a). In order to accommodate tapered balun,

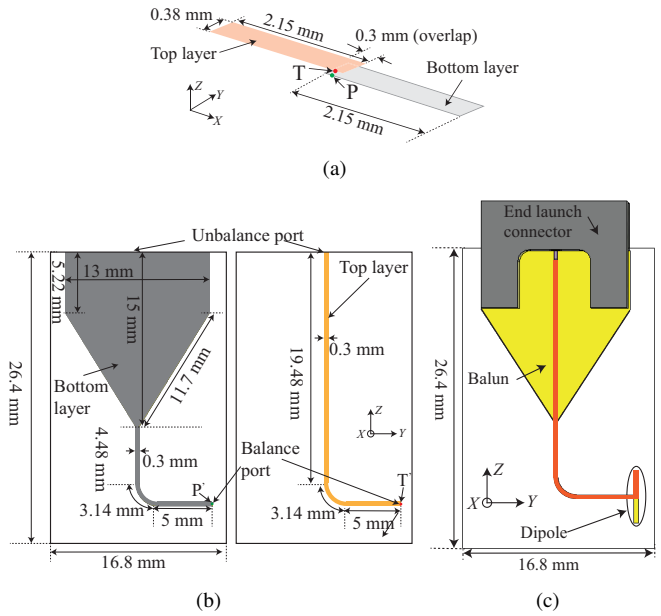

Fig. 1. Electric dipole: (a) vertically polarized half-wavelength dipole, (b) microstrip tapered balun structure, and (c) dipole antenna with the integrated balun.

radiating arms of the proposed dipole utilize both sides of a substrate. One of the dipole arms was patterned on top side of a 127 μm thick substrate RT/duroid 5880 with relative permittivity, $\varepsilon_{\rm r}$, and loss tangent, $\tan\delta$ of 2.2 and 9.0×10^{-4}, respectively. Another arm was printed on the back side of the substrate. Copper of 17 μm thickness was used as a conductor material on the substrate. Length of each dipole arm was approximately 0.25λ at 28 GHz, whereas width was 0.38 mm.

Since the dipole is a balanced antenna, a balun is needed as a feeding network in order to avoid the possible problem caused by the interaction between the balanced antenna and unbalanced coaxial cable. A top metal line and bottom tapered ground plane with an overlapped coplanar stripline (CPS) act as a balun transition to provide a balanced equal power output at the dipole antenna feeding points T′ and P′ as illustrated in Fig. 1(b). The bottom-tapered ground transition was designed to provide an impedance matching tuner with balanced output. The optimization of the feeding network with the tapered balun transition was performed by varying the angle of the tapered ground plane for impedance matching and balanced output. In order to avoid the impact of the balun on the radiation pattern in the azimuth plane, the balun structure was rotated along Z-axis (see Fig. 1(b)). Antenna design and simulation was performed using CST Microwave studio 2018.

The designed dipole and microstrip tapered balun was integrated as illustrated in Fig. 1(c). The balanced port (T′ in Fig. 1(b)) of the top layer of the balun was connected to the top dipole arm (T in Fig. 1(a)). Similarly balanced port P′ in Fig. 1(b) was attached to the bottom dipole arm (P in Fig. 1(a)). The total size of the dipole is 26.4 mm × 16.8 mm.

B. Loop and Microstrip Tapered Balun

One of the main objectives in the design of the loop antenna is to obtain maximum radiation in the plane of its wires

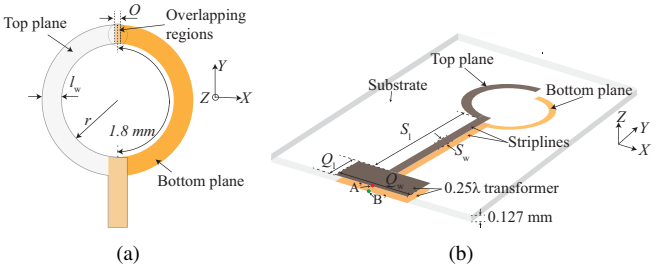

Fig. 2. Loop antenna: (a) geometry of the loop structure, and (b) loop with striplines and quarter-wave impedance transformer.

with nulls broadside to the wires. This goal can be achieved using an electrically small antenna (typically circumference, $C<\lambda/10$). A small loop antenna at 28 GHz needs to have $C = 1$ mm, which is difficult to implement in practice. Therefore, it is necessary to increase the size of the loop without compromising to radiation performance, in particular, radiation pattern. In this paper, we proposed a printed loop with $C = 0.51\lambda$. The loop was patterned on the same substrate as used for the dipole in Section II-A. The inner radius (r) and width of the circular strip ($l_{\rm w}$) were 0.573 and 0.3 mm, respectively. The full circular strip was divided into two half-circles. One of the half-loop arms was printed on the top plane of the substrate, whereas the second half-loop was patterned on the bottom side as shown in Fig. 2(a). Since further increase of the loop size was not possible, striplines were added as illustrated in Fig. 2(b) as tuning parameters. Furthermore, a quarter-wave impedance transformer was implemented to match the antenna.

A 0.51λ loop antenna exhibits a small radiation resistance and large inductive reactance. A series of simulation have performed by varying length ($S_{\rm l}$) and width ($S_{\rm w}$) of the striplines, width of the circular loop strip ($l_{\rm w}$) of the strip, and overlapping regions (O) between the top and bottom loop arms (see Fig. 2(a)) in order to make reactance part close to zero. For $S_{\rm l} = 6.02$, $S_{\rm w} = 0.3$, $l_{\rm w} = 0.3$, and $O = 0.082$ mm, the simulated input impedance of the loop is presented in Fig. 3. The reactance and resistance part of the input impedance at 28 GHz were 0.17 and 3.5 Ω, respectively. A quarter-wave impedance transformer was added at the end of the striplines to achieve 50 Ω matching of the real part. The width ($Q_{\rm l}$) and length ($Q_{\rm w}$) of the transformer was 2.3 and 1.433 mm, respectively. The simulated reflection coefficient of the loop with and without quarter-wave transformer is presented in Fig. 4. As expected antenna without transformer is very poor, while with the transformer the antenna resonates exactly at 28 GHz with $|S_{11}|$ of −22 dB. The simulated −10 dB impedance bandwidth was 0.2 GHz (ranging from 27.9 to 28.9 GHz).

For the loop, the tapered microstrip line was used to form a balun with parallel striplines. The broadband impedance matching properties of the balun was obtained by utilizing a continuous transmission line taper with its characteristic impedance changing smoothly. The smooth transition from a microstrip line to a parallel stripline operates as a balun, shown in Fig. 5. The width of the bottom conductor change

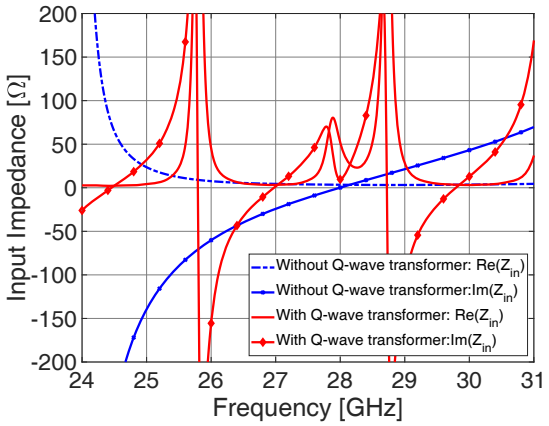

Fig. 3. Simulated input impedance ($Z_{\text{in}} = R_{\text{in}} + jX_{\text{in}}$) of the loop antenna with and without Q-wave transformer.

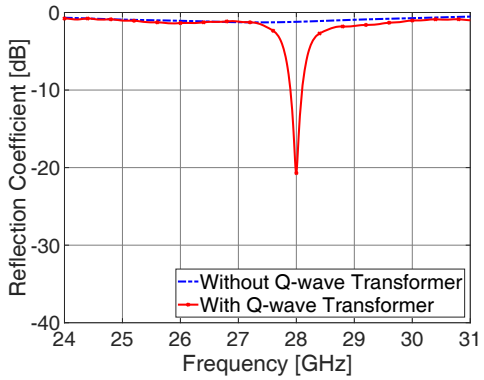

Fig. 4. Simulated reflection coefficient of the loop with and without Q-wave impedance transformer.

gradually corresponding to the line impedance, as visualized in Fig. 5. The length (B_{l}) of the balun was 35.2 mm, whereas width (B_{wc}) at the unbalanced side of the ground plane was tapered from 4.07 to the width (B_{wa}) at the balanced side of 0.376 mm. The exponentially tapered microstrip structure was constructed using loft function in CST Microwave studio 2018 with smoothness factor of 0.25. The balun was simulated with Port-1 and Port-2 at the unbalanced and balanced sides, respectively. The simulated S-parameters of the balun are shown in Fig. 6. The balun shows wideband characteristics. The simulated $|S_{11}|$ less than -10 dB was achieved from 20 to 35 GHz, while insertion losses were less than 0.5 dB for a wide range of frequency bands. With the simulated radiation efficiency of the balun was -18 dB at 28 GHz, the balun mostly transfers power from unbalanced to balanced port rather than radiation. Thus with its wideband behaviors in terms of matching, small insertion loss as well as small radiation the designed balun is suitable to be used for our proposed loop antenna.

The designed microstrip to parallel stripline balun was integrated with the loop antenna as a feeding network. The balanced end ponit A of the baluns' top layer (see Fig. 5) was connected to the top layer of the balanced antenna input point A′ in Fig. 2(b), while for the bottom layer, the points B and

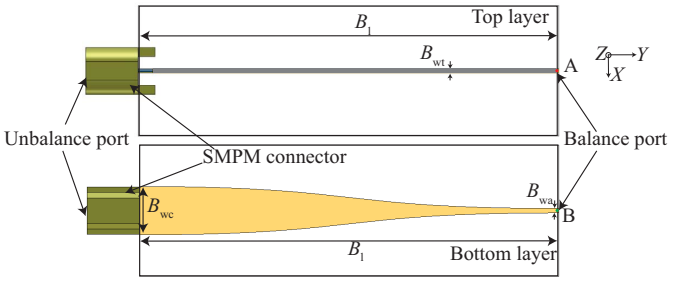

Fig. 5. A single microstrip to parallel striplines balun with an SMPM connector.

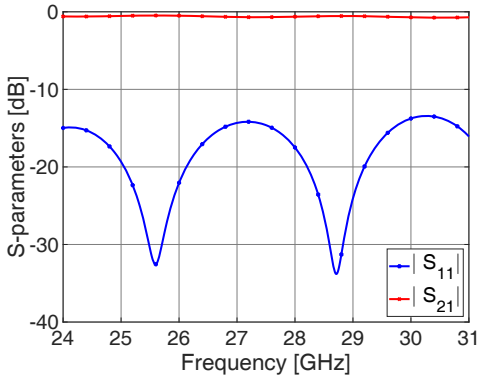

Fig. 6. Simulated S-parameters results microstrip to parallel striplines balun.

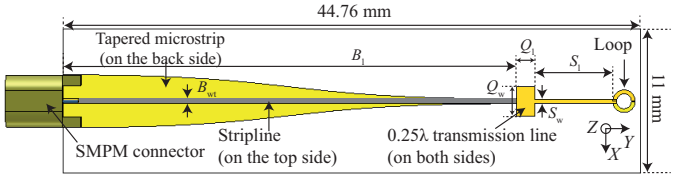

Fig. 7. An illustration of the loop antenna integrated with microstrip tapered balun.

B′ in Fig. 5 and Fig. 2(b), respectively. The proposed loop antenna with integrated tapered balun as a feeding network and SMPM connector is shown in Fig. 7. The total size of the loop is 44.76 mm $\times$ 11 mm.

C. Numerical Results

The simulated reflection coefficients of the dipole and loop integrated with balun are presented in Fig. 8. Note that an end launch and an SMPM connector at the unbalanced side of the balun were included in the simulation for dipole and loop, respectively. Wideband impedance matching has been achieved for the dipole. The loop resonates at 28 GHz with $|S_{11}|$ of -25 dB. The simulated -10 dB impedance bandwidth was 0.2 GHz (from 27.9 to 28.1 GHz) as without balun (see Fig. 4). Fig. 9 shows the the XY-plane cut (coordinate system defined in Fig. 1(c) and Fig. 7 for the dipole and loop, respectively) of the simulated far-field realized gain patterns of co- and cross-polarization for the dipole and loop at 28 GHz. The results show that dipole and loop have a fairly omni-directional radiation pattern on the azimuth plane. The loop

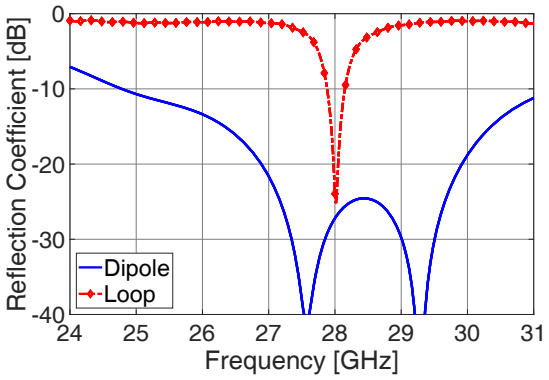

Fig. 8. Simulated reflection coefficients of the dipole and loop antenna.

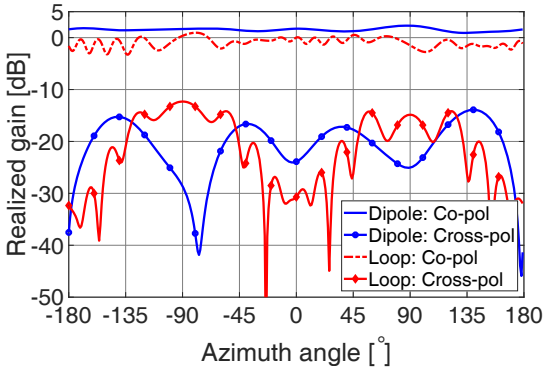

Fig. 9. Simulated radiation pattern of the dipole and loop, XY-plane cut, coordinate system defined in Fig. 1(c) and Fig. 7 for the dipole and loop, respectively.

exhibits more fluctuations in the pattern than dipole due to the presence of the quarter-wave transformer and balun network, which are on the same plane as the loop (i.e., XY-plane). However, the fluctuation in the gain pattern was within 0.7 and 2.1 dB for the dipole and loop, respectively, whereas the maximum simulated realized gain was 2.3 and 1.0 dBi at 28 GHz.

III. Measurements

A. Matching

Fabricated dipole and loop antennas with connector are shown in Fig. 10(a) and Fig. 10(b), respectively. The antenna was connected with a network analyzer (Keysight N5225A PNA) for matching measurements. Comparisons between simulated and measured reflection coefficients are shown in Figs. 11 and 12, respectively. The dipole shows a quite good agreement of shape of curves between simulated and measured reflection coefficients. though they deviate in terms of magnitude. A wideband impedance matching is achieved. The resonance of the loop in the measurement shifts slightly towards a higher frequency at 28.6 GHz compared to simulation. The loop operates well between 28.3 to 28.8 GHz with return loss lower than -10 dB. The difference of the measured results compared to the simulations are probably due to the improper soldering between the antenna and the SMPM connector as well as fabrication inaccuracy.

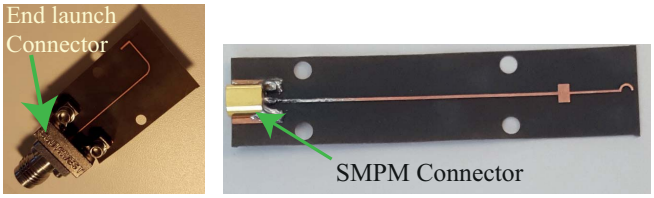

(a) (b)

Fig. 10. Top view of fabricated antennas: (a) dipole with end launch connector, and (b) loop with SMPM connector.

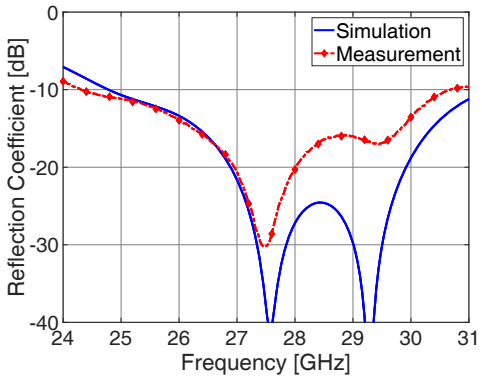

Fig. 11. Simulated and measured reflection coefficient of the vertically polarized dipole; simulated curve is same as in Fig. 8.

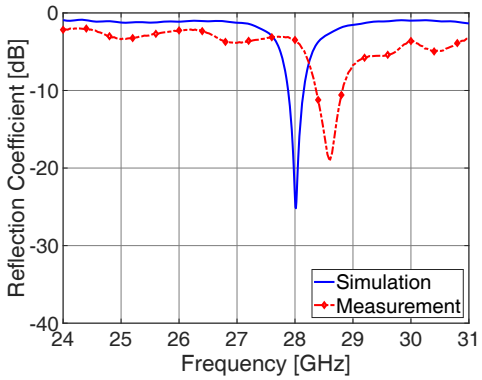

Fig. 12. Simulated and measured reflection coefficient of the loop; simulated curve is same as in Fig. 8.

B. Radiation Pattern

The far-field pattern of the antenna was determined by near-field (NF) measurement. The setup is shown in Fig. 13. The NF was measured at a distance of 24 mm with an open-ended waveguide as the probe. Since the NF measurement system uses a planar field scanner, we measured a part of the full pattern, i.e., from $-45°$ to $45°$ for both azimuth and elevation planes. The gain was determined by comparison with a reference horn antenna at 28 GHz. The azimuth, i.e. XY-plane cut of the simulated and measured realized gain pattern of the dipole and loop are shown in Fig. 14. Fairly omni-directional radiation pattern has been achieved for the dipole. The maximum measured realized gain was 1.5 dB, which is 0.3 dB less compared to the simulation for this region of the pattern. The fluctuations in the pattern are most likely due to the reflection from the antenna fixture as well as

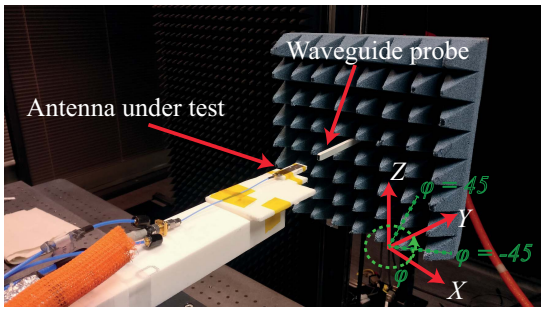

Fig. 13. Antenna in the measurement setup.

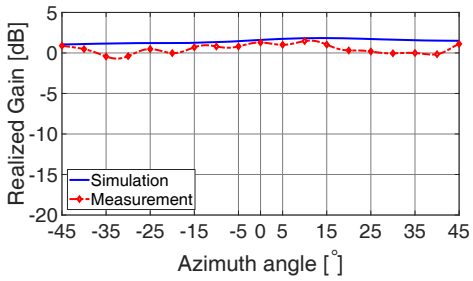

(a)

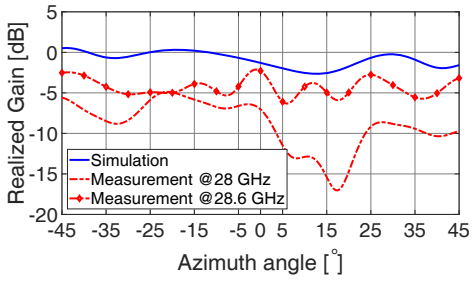

(b)

Fig. 14. Measured and simulated realized gain pattern (azimuth cut): (a) dipole, and (b) loop.

from surrounding objects. Even though the loop was designed to demonstrate omni-directional pattern at 28 GHz center frequency, the measured resonance frequency of the loop was observed at a slightly higher frequency of 28.6 GHz as shown in Fig. 12. We measured the radiation pattern of the loop at both frequencies of 28 and 28.6 GHz. From Fig. 14(b), we can see that the measured realized gain of the loop at 28 GHz is small and the pattern has more fluctuations, which are expected as antenna matching is poorer at this frequency. The measured pattern at 28.6 GHz has similar kind of shape as the simulation but deviates in terms of realized gain values by 2.5 dB within the considered region of the pattern. The fluctuation in the measured gain pattern was 2.1 dB. The lower measured gain compared to the simulation possibly due to the inaccuracy in the fabrication of the antenna and measurements, losses in the substrate, and soldering imperfection of the connector to the antenna.

IV. Conclusion

A dual-polarized omni-directional antenna array is designed in this paper. A printed microstrip dipole and loop with an integrated tapered balun structure is used to form an array. The design and experimental results of low profile microstrip dipole and loop antenna show wideband matching and good radiation performance. The dipole shows -10 dB impedance matching across the bandwidth over 6 GHz, whereas the loop shows 0.2 GHz (from 27.9 to 28.1 GHz). A fairly good agreement between the simulated and measured radiation pattern validates the omni-directional behaviors of both dipole and loop antennas. The dipole and loop have a realized gain of 2.3 and 1 dBi in the simulation. With its fairly omni-directioanl radiation pattern and wideband matching bandwidth, our proposed antenna array can be used to measure omni-directional pathloss as a reference antenna for over-the-air antenna testing. Our future works include the far-field measurement in an anechoic chamber in order to obtain a full 3D pattern in a controlled environment.

References

[1] 3GPP, TR 38.901 (V14.3.0), "Study on channel model for frequency spectrum from 0.5 to 100 GHz," http://www.3gpp.org/dynareport/38901.htm, Dec. 2017.

[2] J. Hejselbaek, J. Ø. Nielsen, W. Fan, and G. Pedersen, "Measured 21.5 GHz indoor channels with user-held handset antenna array," *IEEE Trans. Ant. and Propag.*, vol. 65, no. 12, pp. 6574–6583, Dec. 2017.

[3] I. Syrytsin, S. Zhang, G. F. Pedersen, K. Zhao, T. Bolin, and Z. Ying, "Statistical investigation of the user effects on mobile terminal antennas for 5G applications," *IEEE Trans. Ant. and Propag.*, vol. 65, no. 12, pp. 6596–6605, Dec. 2017.

[4] K. Zhao, J. Helander, D. Sjberg, S. He, T. Bolin, and Z. Ying, "User body effect on phased array in user equipment for the 5G mmWave communication system," *IEEE Ant. and Wireless Propag. Lett.*, vol. 16, pp. 864–867, 2017.

[5] K. Haneda, M. Heino, and J. Jaervelaeinen, "Total array gains of millimeter-wave mobile phone antennas under practical conditions," in *IEEE 87th Vehicular Technol. Conf. (VTC Spring)*, June 2018, pp. 1–6.

[6] A. Clavin, "A new antenna feed having equal E-and H-plane patterns," *IRE Trans. Ant. Propag.*, vol. AP-2, pp. 113–119, Apr. 1954.

[7] M. Li and K. M. Luk, "A differential-fed magneto-electric dipole antenna for UWB applications," *IEEE Trans. Ant. and Propag.*, vol. 61, no. 7, pp. 92–99, Jan 2013.

[8] K. M. Luk and H. Wong, "A differential-fed magneto-electric dipole antenna for UWB applications," *Int. J. Microwaves Opt. Technol.*, vol. 1, pp. 35–44, Apr 2006.

[9] S. Gupta, L. J. Jiang, and C. Caloz, "Magnetoelectric dipole antenna arrays," *IEEE Trans. Ant. and Propag.*, vol. 62, no. 7, pp. 3613–3622, July 2014.

[10] G. Chen and J. Sun, "A printed dipole antenna withmicrostrip tapered balun," *Microwave Opt. Tech. Let.*, vol. 40, no. 4, p. 344 346, Feb. 2004.

[11] T. G. Vasiliadis, E. G. Vaitsopoulos, and G. D. Sergiadis, "A wideband printed dipole antenna with optimized tapered feeding balun for ISM and FWA bands," *Microwave Opt. Tech. Let.*, vol. 43, no. 4, 2004.

[12] A. R. Behera and A. R. Harish, "A novel printed wideband dipole antenna," *IEEE Trans. Ant. and Propag.*, vol. 60, no. 9, pp. 4418–4422, Sept 2012.

[13] K. Meelarpkit, M. Chongcheawchamnan, C. Phongcharoenpanich, M. Krairiksh, L. B. Lok, and I. D. Robertson, "Dual-band microstrip-to-coplanar strip balun transition and loop antenna application," *IET Microwaves Ant. Propag.*, vol. 2, no. 8, pp. 823–829, Dec. 2008.

[14] X. Bai, X. M. Zhang, L. Li, Q. Yang, and J. Y. Li, "Double-sided printed four rhombic-loop antenna with parasitic loops for circular polarization," *J. Electromag. Waves and Applications*, vol. 23, no. 13, pp. 1795–1802, Apr. 2012.

[15] H. Lee, "CPW-fed to CPS dipoleantenna of microstrip tapered balun with triangular loop director," *J. Electro. Eng. Technol.*, vol. 9, no. 4, Apr. 2014.